**Advances in Concrete Construction**, *Vol. 7, No. 2 (2019) 117-126*
DOI: https://doi.org/10.12989/acc.2019.7.2.117


# Post-yielding tension stiffening of reinforced concrete members using an image analysis method with a consideration of steel ratios

Jong-Han Lee[1a], Chi-Young Jung[2b], Tae-Ryeon Woo[3c] and Jin-Hwan Cheung[*3]

[1]*Department of Civil Engineering, Inha University, Incheon, 22212, Republic of Korea*
[2]*Seismic Simulation Test Center, Pusan National University, Yangsan, 50612, Republic of Korea*
[3]*Department of Civil Engineering, Pusan National University, Busan, 46241, Republic of Korea*

*(Received June 1, 2018, Revised March 13, 2019, Accepted March 20, 2019)*

**Abstract.** When designing reinforced concrete (RC) members, the rebar is assumed to resist all tensile forces, but the resistance of the concrete in the tension area is neglected. However, concrete can also resist tensile forces and increase the tensile stiffness of RC members, which is called the tension stiffening effect (TSE). Therefore, this study assessed the TSE, particularly after yielding of the steel bars and the effects of the steel ratio on the TSE. For this purpose, RC member specimens with steel ratios of 2.87%, 0.99%, and 0.59% were fabricated for uniaxial tensile tests. A vision-based non-contact measurement system was used to measure the behavior of the specimens. The cracks on the specimen at the stabilized cracking stage and the fracture stage were measured with the image analysis method. The results show that the number of cracks increases as the steel ratio increases. The reductions of the limit state and fracture strains were dependent on the ratio of the rebar. As the steel ratio decreased, the strain after yielding of the RC members significantly decreased. Therefore, the overall ductility of the RC member is reduced with decreasing steel ratio. The yielding plateau and ultimate load of the RC members obtained from the proposed equations showed very good agreement with those of the experiments. Finally, the image analysis method was possible to allow flexibility in expand the measurement points and targets to determine the strains and crack widths of the specimens.

**Keywords:** tension stiffening; post-yielding; reinforced concrete; image analysis; steel ratio

## 1. Introduction

In reinforced concrete (RC) members, the concrete is resistant to compression but very weak against tension. When designing RC members, the rebar is assumed to resist to all tensile forces by neglecting the cross section of the concrete in the tensile area. However, concrete also resists the tensile forces before a crack occurs. In crack locations, the rebar transmits the tensile stresses over cracks with bond stresses between the rebar and concrete. This increases the tensile stiffness of RC members. Therefore, the tensile stiffness of RC members tends to be higher than that of bare rebar, which is called the tension stiffening effect (TSE).

The ultimate behavior of the RC members is significantly influenced by the increase in the stiffness due to the TSE and the change in the local stiffness due to the occurrence of cracks. The tensile behavior of the RC member converges gradually to that of bare rebar after the concrete cracks occur, which is indicated in design specifications, such as CEB-FIP Model Code 20100 (MC2010), Eurocode 2 (EC2), and British standards BS 8110-1997. The specifications also explain that there is no difference in the tensile behavior between the RC member and the bare rebar after yielding of the rebar. Therefore, previous studies have accounted for the TSE of RC structures only until the yielding of the rebar. However, the tensile force is still transferred to the cracked concrete due to its adhesion with the rebar, even after a crack occurs (Watstein and Parsons 1943, Allam *et al*. 2012, 2013). The TSE was estimated with an empirical value by many researchers. Welch and Janjua (1971) calculated the average steel strain $\varepsilon_{sm}$ as Eq. (1).

$$\varepsilon_{\mathrm{sm}} = (f_s - 20.7)/E_s \quad (1)$$

The value of 20.7 is the empirical value of tension stiffening which is approximately equal to $f_{ct}E_s/E_c$. Where $f_{ct}$ is the tensile strength of the concrete, $E_s$ and $E_c$ are the elastic modular of rebar and concrete, respectively. Gergely and Lutz (1968) assumed that the concrete tension stiffening is not affected by the steel stress when the stabilized crack pattern has been formed. Therefore, in the cracked stage, the tension stiffening is a constant value and is affected only by the concrete tensile strength and the bond behavior between the steel and concrete at the tensioned region of the section, regardless the steel stress level.

Leonhardt (1977) presented a model for computing the mean strains. The average strain over the entire length,

∗Corresponding author, Professor
E-mail: cheung@pusan.ac.kr
[a]Professor
E-mail: jh.lee@inha.ac.kr
[b]Ph.D.
E-mail: cyjung@pusan.ac.kr
[c]Ph.D. Student
E-mail: wootaelyeon@pusan.ac.kr



ISSN: 2287-5301 (Print), 2287-531X (Online)

$\varepsilon_{sm}$, is less than the bare rebar strain, $\varepsilon_s$, which is the strain developed by the rebar alone after cracking. The differences between $\varepsilon_{sm}$ and $\varepsilon_s$ is referred to as TSE. If the cracking strain of the concrete, $\varepsilon_{cm}$, is ignored as being very small, $\varepsilon_m$ may be approximated by Eq. (2).

$$\varepsilon_m = \varepsilon_{sm} = \varepsilon_s \left(1 - \left(\frac{f_{scr2}}{f_s}\right)^2\right) \quad (2)$$

where $f_s$ is the stress in the tension reinforcement assuming a cracked section, $f_{scr2}$ is the rebar stress after cracking (2008).

If the TSE is neglected in the design of a structure, the amount of rebar required can be overestimated. Accurate estimation of the stiffness of concrete structures can be important for a number of reasons. In general, these reasons are related to the serviceability and occasionally the constructability of the structure. In several cases where stiffness governs the load distribution, the ultimate limit state may also be affected. TSE has a relatively minor effect on the deformation of heavily reinforced members but is highly significant in lightly reinforced members. If the TSE is disregarded, the stress of the rebar can be considerably overestimated, which can result in underestimation of the safety of RC structural members, such as panel, slab, and shell structures (Balazs 1993, Yankelevsky *et al*. 2008, Lee and Cho 2011a, 2011b, Scott and Beeby 2012, Lee and Cho 2013, Mondal and Prakash 2015).

Yankelevsky *et al*. (2008) developed a one-dimensional model to simulate the tension stiffening of cracked concrete. They formulated the analytical relationships in terms of the stiffness of concrete-rebar composite and predicted the stress, strain, and displacement fields in the concrete along the rebar. Lee *et al*. (2011a) evaluated the contribution of concrete TSE to the post-yielding deformation response of RC members and formulated a simplified constitutive model using analytical parametric studies. They determined the influence of various parameters, including the concrete compressive strength, rebar yield strength, ultimate strength, hardening stress, and hardening strain. Scott and Beeby (2012) discussed the importance of deflection control in RC structures and emphasized a number of problems that could affect the accuracy of deflection calculations.

Lee *et al*. (2011b) conducted analytical parametric studies to determine the influence of various parameters including concrete compressive strength and rebar yield strength, ultimate strength, hardening stress, and hardening strain. The model was proposed to be able to estimate the reduced ductility of the RC member. The proposed model makes it possible to accurately calculated rebar stresses at crack locations and average strain conditions which result in rupture of rebar.

This study estimates the change of TSE after yielding of rebar and investigates the effect of the steel ratio on the TSE. RC member specimens were fabricated for uniaxial tensile tests using steel ratios of 2.87%, 0.99%, and 0.59%. A vision-based non-contact measurement system was used to measure the behavior of the specimens. The vision-based system has been effectively applied to measure the displacements and strains in civil and architectural engineering applications (Lee *et al*. 2012, Fukuda *et al*. 2013, Ye *et al*. 2013, Lin 2015, Feng and Feng 2016, Ye *et al*. 2016, Kang *et al*. 2017). The image processing algorithm involved in this study is based on the color information of several reference objects in the Lab color space. In addition, a load indicator that is wirelessly connected to a data logger system on the main server was applied to synchronize it with the time of the captured targets. In the post-processing step, the strains and load were analyzed to evaluate the TSE and ductility of the RC member. The relationship between the TSE and steel ratio of the RC members was analyzed to determine the post-yielding TSE of the RC members. The results are distinguished from MC2010 in that MC2010 only accounts for the TSE until the yielding point. Based on the experimental results, empirical equations are proposed to estimate the TSE from the yielding to limit states.

## 2. Tension stiffening effect

A main study on the TSE in the RC members was performed by Johnson (1951), who proposed a stress-strain relationship to explain the effect. The theoretical equation, proposed by Johnson (1951), has been adopted in MC2010 and EC2 as the function of the mean strain of concrete and rebar. Several studies have also proposed empirical models for the prediction of the TSE in RC members. Collins and Mitchel (1991) used the mean tensile stress of concrete after cracking to evaluate the TSE. Belarbi and Hsu (1994) evaluated the mean strain function of TSE, which is obtained from the stress-strain relationship between concrete and rebar.

### *2.1 CEB-FIP Model Code 2010 (MC2010)*

MC2010 separates the behavior of an RC member into four stages based on the cracking of the concrete and the yielding of the bar. After concrete cracks occur, the load is transferred from the rebar to concrete by the bond stresses at their interface in the stabilized crack stage. The concrete resists a part of the transferred load. Therefore, the strain in the rebar of an RC member is smaller than that in bare rebar. In the crack formation stage the normal tensile force does not increase, because it falls back after the occurrence of any new crack. If so many cracks have been formed that there are no undisturbed areas left the tensile strength of the concrete cannot be reached anymore between the cracks, so no new cracks will appear. After this phenomenon the stabilized cracking stage will be started. In the stabilized cracking stage the existing cracks widen. Finally, the rebar will start yielding. For the crack formation stage the constant tensile cracking force, $N_r$, can be expressed by Eq. (3). The crack formation stage applies when, for imposed deformation, the strain satisfies the Eq. (4).

$$\mathrm{N_r} = A_c f_{ctm}\left(1 + \alpha_e \rho_{s,ef}\right) \quad (3)$$

$$\varepsilon \leq \frac{f_{ctm}\cdot(0.6+\alpha_e)}{E_s \cdot \rho} \quad (4)$$

where $\alpha_e = E_s/E_c$ is modular ratio, $\rho_{s,eff}$ is effective

reinforcement ratio for tensile bar, and $N_r$ is tensile force at which cracking occurs. The mean rebar strain can be expressed by

$$\varepsilon_{s,m} = \varepsilon_{so} - \beta_{t,m}\Delta\varepsilon_{sr} = \varepsilon_{so} - \beta_{t,m}(\varepsilon_{sr2} - \varepsilon_{sr1}) \quad (5)$$

where $\beta_{t,m}$ is an integration factor for the rebar strain along the transmission length, $\varepsilon_{s,m}$ is the mean rebar strain, $\varepsilon_{so}$ is the strains of the rebar in cracked concrete, $\varepsilon_{sr1}$ and $\varepsilon_{sr2}$ are the rebar strains at the point of zero slip and the crack under the cracking force, respectively, and $\Delta\varepsilon_{sr}$ is the increase of the rebar strain in the cracking state.

After the crack formation, the transferred bond force reduces with decreasing transmission length. The reduction of the rebar strain from the crack to the middle point between the cracks, $\Delta\varepsilon_{s,m}$, can be calculated using Eq. (6). The mean strain over the total member, $\varepsilon_{s,m}$, is obtained using Eq. (7).

$$\Delta\varepsilon_{s,m} = \frac{2}{3}\Delta\varepsilon_{sr} \quad (6)$$

$$\varepsilon_{\mathrm{s,m}} = \varepsilon_{\mathrm{s2}} - \beta_{t,m}\Delta\varepsilon_{s,m} = \varepsilon_{s2} - \beta_t\Delta\varepsilon_{sr} \quad (7)$$

where $\beta_t = \frac{2}{3}\beta_{t,m}$, which is equal to 0.4 for instantaneous loading and 0.25 for long-term and repeated loadings.

### *2.2 Eurocode 2 (EC2)*

In EC2, the TSE is defined using the mean strain of an RC member after cracks, similar to MC2010. EC2 calculates the crack width of a flexural member using the following equation

$$(\varepsilon_{\mathrm{sm}} - \varepsilon_{cm}) = \frac{\left(f_s - K_t\left(\frac{f_{cteff}\left(1+n\rho_{eff}\right)}{\rho_{eff}}\right)\right)}{E_s} \geq 0.6\frac{f_s}{E_s} \quad (8)$$

where $K_t$ is a factor expressing the duration of loading (0.6 for short-term loading and 0.4 for long-term loading), and $f_s$ is the stress in the tension rebar, computed based on the cracked section. $n$ is the modular ratio of the rebar to concrete, $f_{cteff}$ is the mean tensile strength of the concrete when the crack first occurs, and $\rho_{eff} = \frac{A_s}{A_{ceff}}$, which is the ratio of the area of the tension rebar to the effective tension area of the concrete surrounding the tension rebar. Therefore, $(\varepsilon_{sm} - \varepsilon_{cm})$ in Eq. (8) represents the difference of the mean tensile strains of the rebar and concrete, and thus, the term $\frac{K_t\left(\frac{f_{cteff}\left(1+n\rho_{eff}\right)}{\rho_{eff}}\right)}{E_s}$ represents the TSE in the RC member.

## 3. Experimental program

### *3.1 Test variable and specimens*

Test specimens were manufactured to observe the characteristics of the TSE with different steel ratios. According to MC2010, the rebar is completely restrained in the concrete when the cover thickness of the RC member is more than or equal to five times the rebar diameter. Based on this regulation, specimens were fabricated with steel ratio of 0.59%. The specimens with steel ratio of 2.87% are applied with the cover thickness of the RC member which is built in the normal environmental condition (KHBS 2012). Finally, the steel ratio of 0.99% was selected from among the values between 2.87% and 0.59%. Through the test parameter of theses specimens, it was tried to understand the behavior of the tensile member with a thin cover thickness. Table 1 overviews the features of each specimen. The compressive strength of the concrete was 30 MPa, and the yield strength of the rebar was 400 MPa. Fig. 1 shows the manufacturing process of the specimens.

Table 1 Overview of the features of each specimen

| Component | Bare rebar | Steel ratio | | |
|---|---|---|---|---|
| | | 2.87% | 0.99% | 0.59% |
| Length (mm) | 1,000 | 1,000 | 1,000 | 1,000 |
| Steel grade | SD400 | SD400 | SD400 | SD400 |
| Rebar diameter (mm) | 19.1 | 19.1 | 19.1 | 19.1 |
| Rebar area ($mm^2$) | 286.5 | 286.5 | 286.5 | 286.5 |
| Section area (mm) | - | 100×100 | 170×170 | 220×220 |
| Strength of concrete (MPa) | - | 30 | 30 | 30 |
| Ratio of cover thickness to rebar diameter | - | 2.12 | 3.95 | 5.26 |

(a) Pouring concrete

(b) Curing specimens

Fig. 1 Manufacturing process of the specimens

### *3.2 Test set-up and vision system instrumentation*

The specimens were tested under uni-axial tension using a 1000-kN universal testing machine (UTM). The rebar was exposed at both ends of the specimen and gripped by the UTM. Tensile force was applied to the specimen using the displacement control. The test was performed until the rebar ruptured. Targets were attached to the surface of the

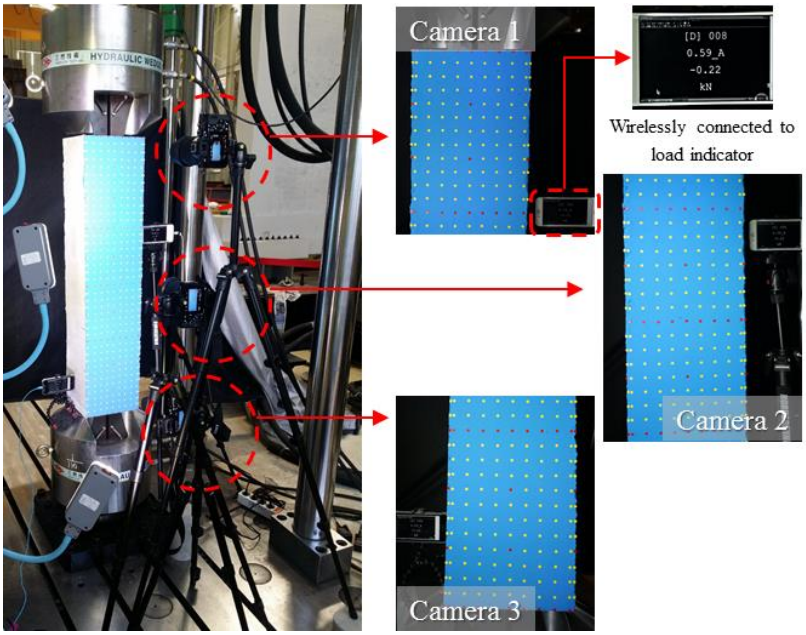


Fig. 2 Instrumentation and measurement of the specimen Mesh grid of topographic model

specimen to measure the displacement and strain of the specimen using an image processing method. The diameter of the target is 5 mm. The targets were arrayed with 25 mm by 25 mm distance. The strains can be calculated from the distances between the targets. Three digital cameras (Sony Alpha 7R) were used to take pictures of the top, middle, and bottom of the specimen. The pictures contained both the targets attached to the specimen and the load indicator.

Both the load and the strain are easily and accurately synchronized using the load indicator and recording the current load value with the target. The object distance from the camera and the image resolution (7360×4912 pixels) were determined to maintain a scale of approximately 0.08 mm/pixel. This means that the measurement resolution obtained from the image processing is approximately 0.08 mm, which is similar to that from a 100-mm linear variable differential transformer (LVDT). Fig. 2 shows the instrumentation and measurement for the experiment.

### *3.3 Vision-based measurement system*

A non-contact image processing method was used to evaluate the displacement of the targets on the specimen. The target recognition algorithm used in image processing significantly affects the accuracy of the analysis results. A conventional target recognition algorithm is based on only the coherence analysis requires a long time for computation for accurate analysis. However, the algorithm used in this study is based on the geometric shape of the objects in addition to coherence analysis of the color information. Using these two types of information reduces the amount of calculation and increases the accuracy of the results. Furthermore, the method can analyze many targets in an image, which reduces the analysis time. Fig. 3 shows the algorithm of the image processing method. The algorithm consists of obtaining an image, converting the image to a binary image, analyzing the binary image to determine the

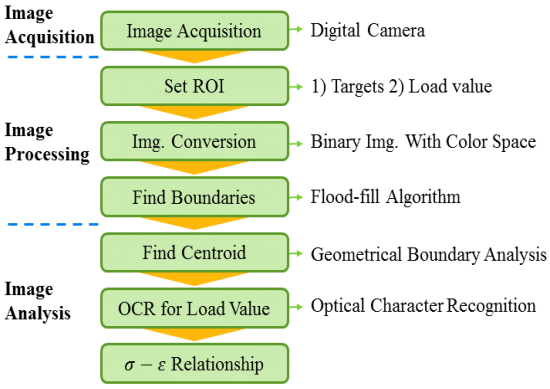


Fig. 3 The algorithm for the image processing method (Lee, 2017)

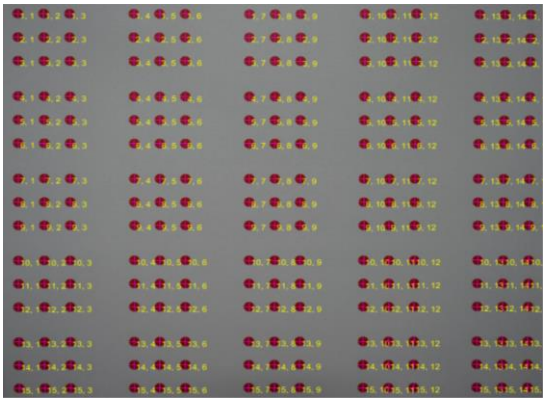

Fig. 4 Image used for evaluating image distortion

centers of the targets, and calculating the strain and load of the specimen (Lee 2017).

To investigate the degree of image distortion of the digital camera used for the image acquisition, targets with a diameter of 5 mm were divided into groups of nine and arranged in 5 rows and 5 columns, as shown in Fig. 4. The

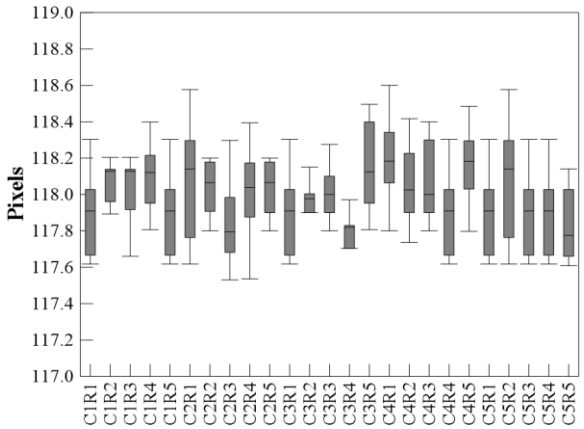


Fig. 5 Deviation of the diameter of the target groups

Table 2 Results of bare rebar specimens

| No. | Yield stress ($f_y$, MPa) | Ultimate stress ($f_u$, MPa) | $f_u/f_y$ | Limit state strain ($\varepsilon_u$) | Fracture strain ($\varepsilon_f$) |
|---|---|---|---|---|---|
| A | 489.18 | 600.24 | 1.23 | 0.111 | 0.119 |
| B | 499.30 | 606.63 | 1.21 | 0.109 | 0.116 |
| C | 496.34 | 602.55 | 1.21 | 0.095 | 0.113 |
| Average | 494.94 | 603.14 | 1.22 | 0.105 | 0.116 |

image was then analyzed using the image processing method. The diameter of the target is expressed as the number of pixels to examine the variance in the diameter according to the location of the targets in the image. Fig. 5 shows the deviation of the target diameters. The number pixels of the 5-mm diameter targets ranged from around 117.5 to 118.5, which means that the average error of the diameter from image distortion is less than 1 pixel. Therefore, the image processing was carried out using the distortion correction function of the digital camera.

## 4. Experimental results and discussion

### *4.1 Load and strain relationship*

The yielding and ultimate loads of bare rebar were first evaluated to determine the relationship between the TSE and steel ratio. Table 2 summarizes the experimental results. The mean yield and ultimate stresses were 494.94 and 603.14 MPa, respectively. The ratio of the ultimate stress to the yield stress was 1.22. The mean limit and fracture strains were 0.105 and 0.116, respectively.

The experimental results of the bare rebar were compared with those of RC members, as shown in Fig. 6. The ductility and yielding plateau of RC members were lower than those of the bare rebar. In addition, the RC members had lower ductility and yielding plateaus as the steel ratio decreased. As the load increased, the number of cracks continued to increase after the initial cracks, and the total number of cracks decreased as the steel ratio increased. The initial cracking load tends to increase as the steel ratio decreases. The initial cracks occurred at the same level of stresses, which were calculated using the transformed section area.

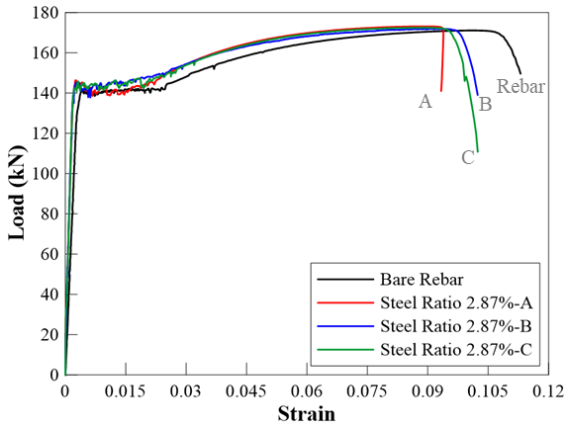


(a) Steel ratio 2.87%

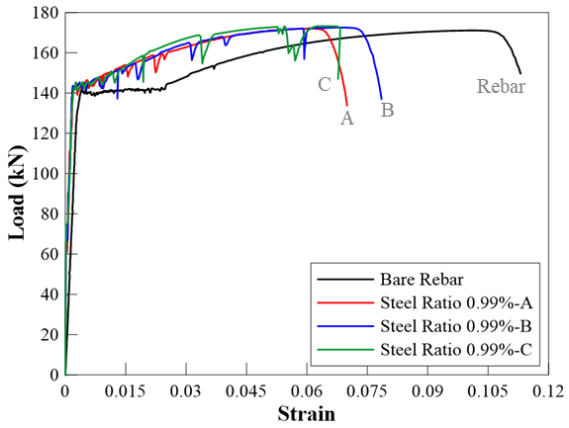


(b) Steel ratio 0.99%

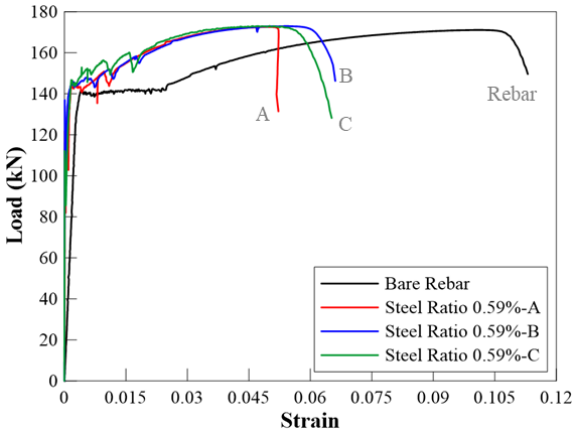


(c) Steel ratio 0.59%

Fig. 6 Load-strain relationship

### *4.2 Effect of steel ratios on the load and strain*

Fig. 7 shows the strain results of the specimens. The ductility and yielding plateau decreased as the steel ratio decreases. The mean limit state and fracture strains of the bare rebar were 0.105 and 0.119, respectively. The mean limit state strains of RC members with steel ratios of 2.87%, 0.99%, and 0.59% were 0.090, 0.064, and 0.051, respectively, while the mean limit state strains were 0.090, 0.064, and 0.051. According to linear regression analysis, the limit state and fracture strains are proportional to the steel ratios, as shown Fig. 8.

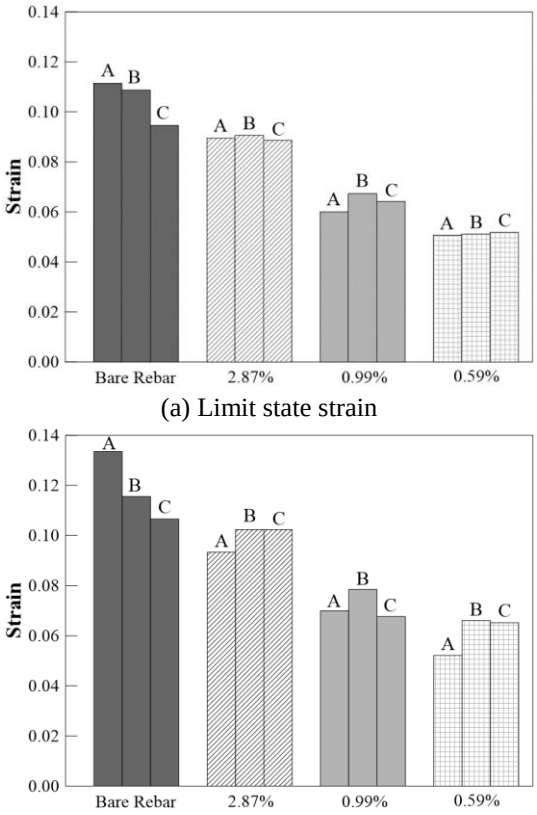


(a) Limit state strain

(b) Fracture strain

Fig. 7 The strain results of the specimens

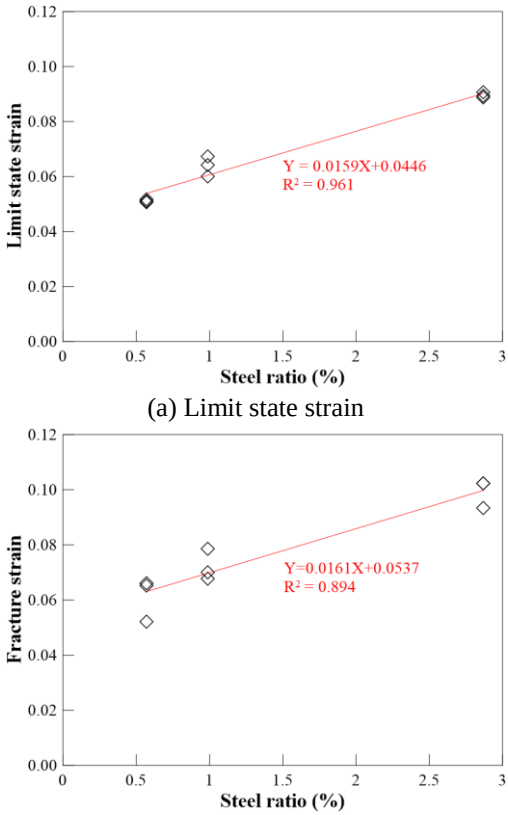


(a) Limit state strain

(b) Fracture strain

Fig. 8 The statistics result of the test results

### *4.3 Crack patterns and crack widths*

Figs. 9 to 11 show the cracks on the specimen at the stabilized cracking stage and the fracture stage. The horizontal axis in the graph over the crack figure means the distance from the left end of the specimen. The vertical axis in the graph is the crack width. The specimens of steel ratio of 2.87% showed the average 8.7 cracks, and the specimens of steel ratio of 0.99% showed the average 6 cracks. The specimens of steel ratio of 0.59% showed the average 2.7 cracks. The results shows that the number of the cracks increases as the steel ratio increases. In the specimens of

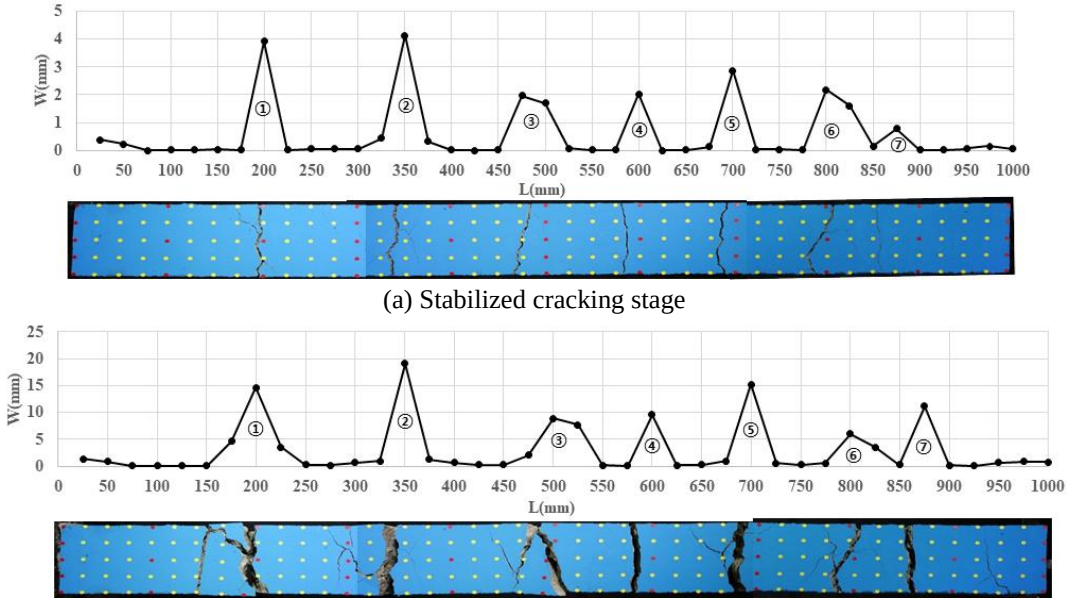


(a) Stabilized cracking stage

(b) Fracture stage

Fig. 9 Crack pattern and crack width (Steel ratio 2.87%)

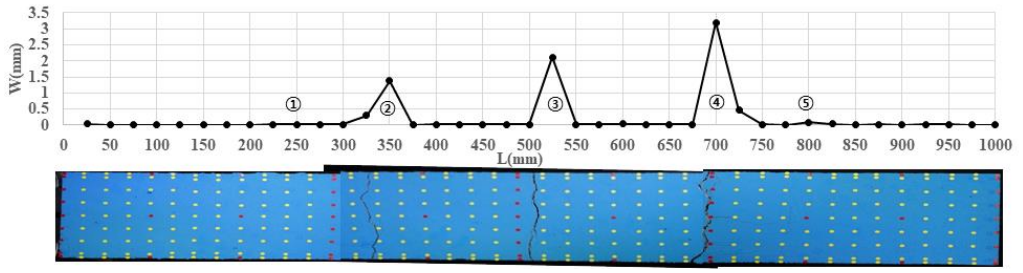


(a) Stabilized cracking stage

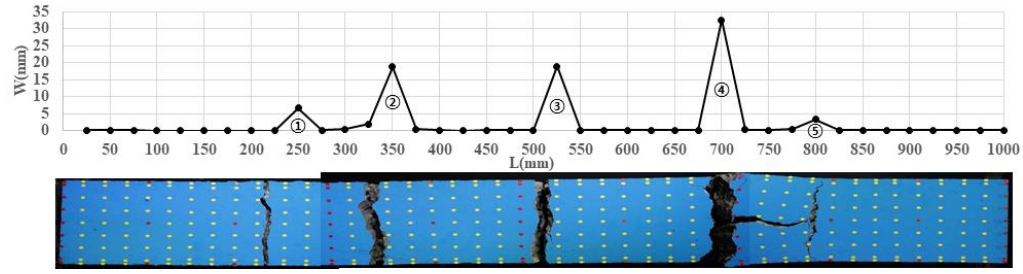


(b) Fracture stage

Fig. 10 Crack pattern and crack width (Steel ratio 0.99%)

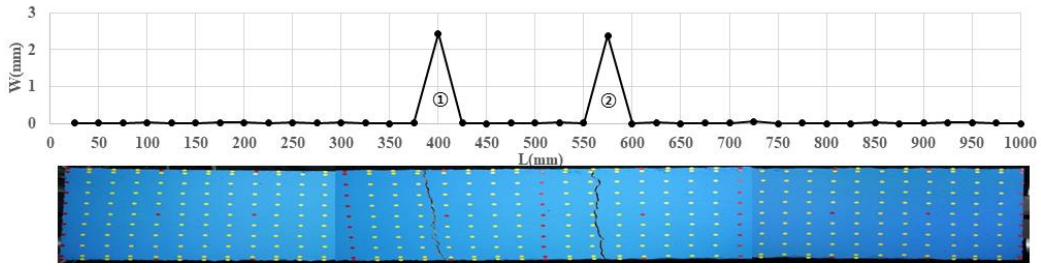


(a) Stabilized cracking stage

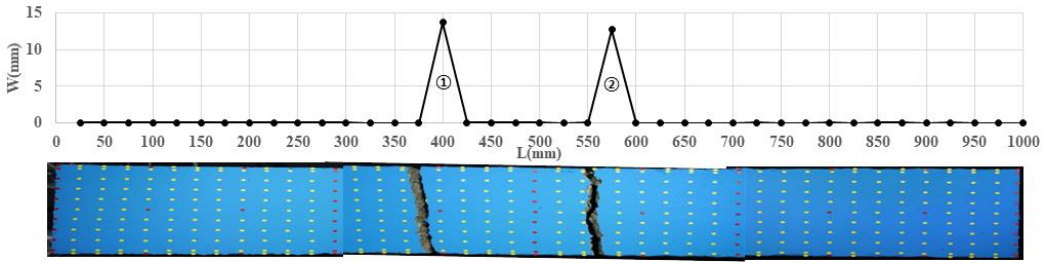


(b) Fracture stage

Fig. 11 Crack pattern and crack width (Steel ratio 0.59%)

steel ratio of 0.59% and 0.99% the splitting cracks occurred at the fracture stage. According to the MC2010, the cover thickness to rebar diameter ratio is related with the splitting cracks. The splitting cracks can affect the behavior by increasing the ductility of the RC member. Usually, the cover thickness of the RC girder can be less than 5 times of the rebar diameter. The tensile part of the RC girder can show the similar behavior with the results of this study. Therefore, the tension stiffening effect after the yield of the rebar should be estimated to analyze the ultimate behavior of the RC girder.

## 5. Evaluation method for the tension stiffening of RC members

### *5.1 Tension stiffening until the yielding of the rebar*

Based on the experimental results, an empirical equation is proposed to estimate the TSE from the yielding to limit states. Fig. 12 shows the load-strain relationships of the specimens until the yielding state. The experimental results were compared with the theoretical results obtained using the equation presented in MC2010. With a steel ratio of 2.87%, the stiffness of RC members from the beginning of the crack formation to the yielding of the rebar was greater than the result of MC2010. The concrete of the RC member had a greater contribution to the stiffness than suggested by MC2010, but the difference between the experimental results and MC 2010 was minimal. For the steel ratio of 0.59%, the load suddenly decreased in the beginning of the

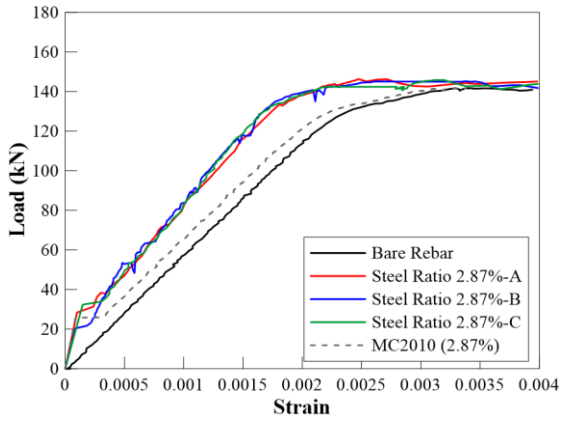


(a) Steel ratio 2.87%

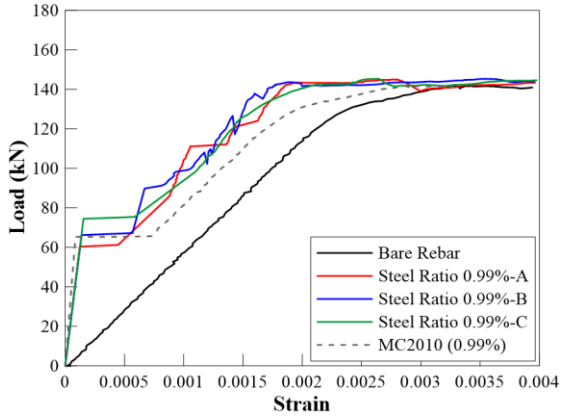


(b) Steel ratio 0.99%

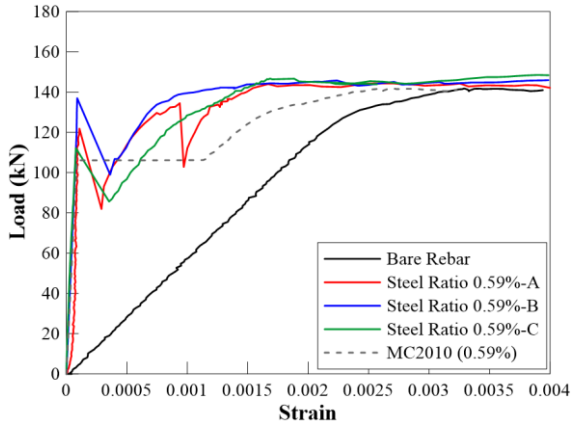


(c) Steel ratio 0.59%

Fig. 12. Comparisons between the experimental results and the results of MC2010 in the load-strain relationship

crack formation stage. In general, the equation proposed in MC2010 showed good agreement with the TSE of the experimental results

### *5.2 Tension stiffening after the yielding of the reinforcement*

As shown in Fig. 6, the ductility of RC members after the yielding of the rebar decreased with decreasing steel ratio. In addition, the reductions of the limit state and fracture strains were dependent on the ratio of the rebar. Therefore, MC2010 is limited in assessing the TSE after the

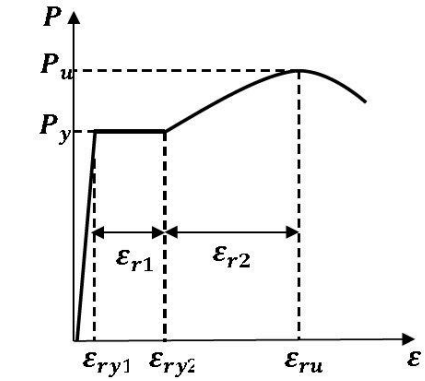


(a) Bare rebar

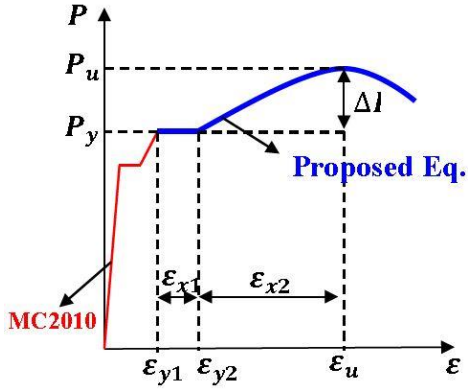


(b) Tension stiffening effect (TSE)

Fig. 13 Notation of the characteristic value in the load-strain relationship

yielding of RC members. To expand the applicability of the TSE equations proposed in MC2010, an empirical equation is proposed to account for the effect of the steel ratio on the TSE after the yielding of an RC member. The new TSE equations also account for the material properties of the rebar, such as the diameter, yield strength and plateau, and ultimate strength.

The TSE after yielding of an RC member was defined using $\varepsilon_{r1}$, $\varepsilon_{r2}$, $\varepsilon_{x1}$, $\varepsilon_{x2}$, and $\Delta P$, shown in Fig. 13. The steel ratio significantly influences the TSE after yielding of the member and was expressed in terms of the yielding plateau and strain hardening. The TSE up to the yielding of the RC member was formulated using MC2010. The resulting TSE equations are as follows

$$\varepsilon_{r1} = \varepsilon_{ry2} - \varepsilon_{ry1} = \frac{0.065}{d^{0.435}} \tag{6}$$

$$\varepsilon_{r2} = \varepsilon_{ru} - \varepsilon_{ry2} \tag{7}$$

$$\varepsilon_{x1} = \varepsilon_{y2} - \varepsilon_{y1} = \varepsilon_{r1} - \frac{0.0016}{\rho^{0.45}} \tag{8}$$

$$\varepsilon_{x2} = \varepsilon_{u} - \varepsilon_{y2} = 2.6\varepsilon_{r2} \cdot \rho^{0.3} \tag{9}$$

$$\Delta P = -\left(5800 + \frac{10}{\rho}\right)\left(\varepsilon - \varepsilon_{y2}\right)^2 + \left(8500 + \frac{1}{\rho}\right)(\varepsilon - \varepsilon_{y2}) \quad (\varepsilon \le \varepsilon_u - \varepsilon_{y2}) \tag{10}$$

where $\varepsilon_{ry1}$ and $\varepsilon_{ry2}$ are the strains at the beginning and end of the yielding plateau of the bare rebar, respectively; $d$ is the diameter of the rebar; $\rho$ is the steel ratio; $\varepsilon_{ru}$ is the limit state strain of the bare rebar, which is obtained

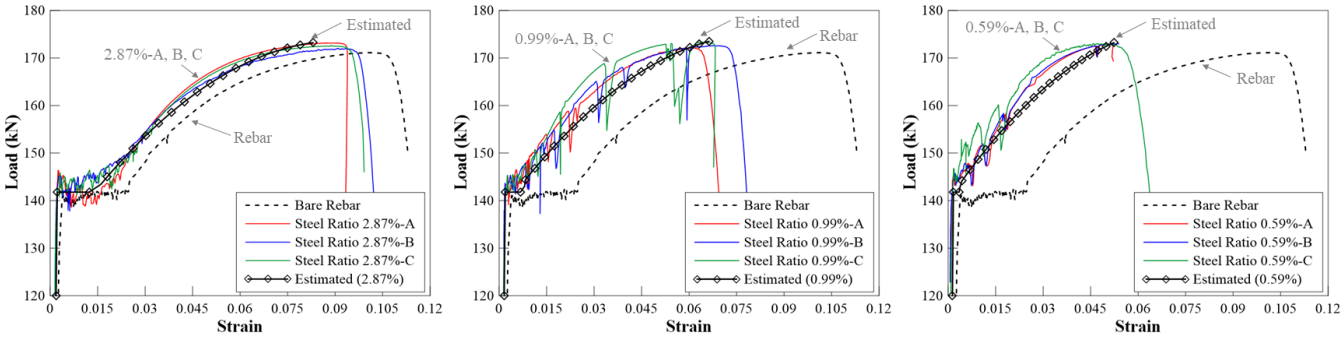


(a) 2.87% (b) 0.99% (c) 0.59%

Fig. 14 Comparison between the experimental results and the result calculated with the proposed equation

Table 3 Comparisons between the experimental results and the estimated results of the TSE of RC members

| Steel ratio (%) | | $\varepsilon_{x1}$ | | | | $\varepsilon_{x2}$ | | | | $\Delta P$ | | | |
|---|---|---|---|---|---|---|---|---|---|---|---|---|---|
| | | Exp. | Prop. | Ratio | Avg. | Exp. | Prop. | Ratio | Avg. | Exp. | Prop. | Ratio | Avg. |
| 2.87 | A | 0.0137 | 0.0101 | 0.737 | 0.730 | 0.0870 | 0.0716 | 0.823 | 0.827 | 22.29 | 31.83 | 1.428 | 1.343 |
| | B | 0.0121 | | 0.834 | | 0.0873 | | 0.821 | | 26.39 | | 1.206 | |
| | C | 0.0163 | | 0.620 | | 0.0855 | | 0.838 | | 22.81 | | 1.395 | |
| 0.99 | A | 0.0047 | 0.0053 | 1.128 | 1.243 | 0.0580 | 0.0521 | 0.898 | 0.847 | 27.14 | 31.70 | 1.168 | 1.133 |
| | B | 0.0038 | | 1.395 | | 0.0655 | | 0.795 | | 28.94 | | 1.095 | |
| | C | 0.0044 | | 1.205 | | 0.0616 | | 0.846 | | 27.94 | | 1.135 | |
| 0.59 | A | 0.0025 | 0.0019 | 0.760 | 0.999 | 0.0469 | 0.0446 | 0.952 | 0.915 | 28.32 | 31.16 | 1.100 | 1.143 |
| | B | 0.0017 | | 1.118 | | 0.0513 | | 0.870 | | 27.22 | | 1.145 | |
| | C | 0.0017 | | 1.118 | | 0.0484 | | 0.922 | | 26.32 | | 1.184 | |
| | | Avg. | | 0.991 | | | | 0.863 | | | | 1.109 | |

from the tensile test; $\varepsilon_{y1}$ and $\varepsilon_{y2}$ are the strains at the beginning and end of the yielding plateau of the RC member, respectively; and $\Delta P$ is the increase of the load from the end of the yielding plateau to the ultimate state of the RC member.

The post-yielding TSE calculated using the proposed equations was compared with the experiments. As shown in Fig. 14, the values of the yielding plateau and ultimate load of the RC members matched very well with the experiments. Table 3 compares the limit state strain and ultimate load obtained from the proposed equations with those of the experiments. The proposed equations exhibited a good estimation of the load-strain relationship of RC members until the ultimate state.

## 6. Conclusions

An experimental investigation was performed to evaluate the ultimate behavior characteristics and TSE of RC members with steel ratios of 2.87%, 0.99%, and 0.59%. Based on the experimental results, the relationship between the TSE and steel ratio of RC members was analyzed to characterize the post-yielding TSE of RC members. The new formulation is distinguished from MC2010, which only accounts for the TSE until the yielding point. Findings and conclusions derived from this study are summarized as follows:

- The reductions of the limit state and fracture strains were dependent on the ratio of the rebar. As the steel ratio decreased, the strain after yielding of RC members decreased significantly. Therefore, the overall ductility of the member is reduced as the steel ratio decreases.
- Based on the experimental results, an empirical equation was proposed to account for the effect of the steel ratio and material properties of the rebar on the TSE from the yielding state to the ultimate state of the member. The yielding plateau and ultimate load calculated using the proposed equations matched very well with the experimental results.
- The cracks on the specimen at the stabilized cracking stage and the fracture stage were measured with the image processing method. The results show that the number of cracks increases as the steel ratio increases.
- In this study the image processing method was used to measure the strains and crack widths of the RC member in tension. It was possible to allow flexibility in expand the measurement points and targets to determine the strains and crack widths of the specimens.

The equations proposed for estimating the TSE are based on experiments for concrete with a compressive strength of 30 MPa and rebar with a yield strength of 400 MPa, which can generally be applied to RC structures. Further studies are recommended using different strengths of concrete and steel grades of rebar. The multiple effect of the cover thickness and steel ratio on the ultimate behavior of the RC member should be considered in the future works.

## Acknowledgments

This research was supported by the Basic Science Research Program through the National Research Foundation of Korea (NRF) and funded by the Ministry of Education (2014R1A1A2058484).

## References

Allam, S.M., Shoukry, M.S., Rashad, G.E. and Hassan, A.S. (2012), "Crack width evaluation for flexural rc members", *Alexandria Eng. J.*, **51**, 211-220.

Allam, S.M., Shoukry, M.S., Rashad, G.E. and Hassan, A.S. (2013), "Evaluation of tension stiffening effect on the crack width calculation of flexural rc member", *Alexandria Eng. J.*, **52**, 163-173.

Balazs, G.L. (1993), "Cracking analysis based on slip and bond stresses", *Am. Concrete Inst.: Mater. J.*, **90**, 320-348.

Belarbi, A. and Hsu, T.T.C. (1994), "constitutive laws of concrete in tension and reinforcing bars stiffened by concrete", *Am. Concrete Inst.: Struct. J.*, **91**, 465-474.

Collins, M.P. and Mitchell, D. (1991), *Prestressed Concrete Structures*, Prentice Hall, New Jersey, UK.

Committee Euro-International Du Beton (2013), CEB-FIP Model Code 2010, Design Code, Thomas Telford, Paris, France.

Eurocode 2 (2010), Design of Concrete Structures-Part 1-1: General Rules and Rules for Buildings, CEN/TC250, EN 1992-1-1.

Feng, D. and Feng, M.Q. (2016), "Vision-based multipoint displacement for structural health monitoring", *Struct. Control Hlth. Monit.*, **23**, 876-890.

Fukuda, Y., Feng, M.Q., Narita, Y., Kaneko, S. and Tanaka, T. (2013), "Vision-based displacement sensor for monitoring dynamic response using robust object search algorithm", *IEEE Sens. J.*, **13**, 4725-4732.

Gergely, P. and Lutz, L.A. (1968), "Maximum crack width in RC flexural members, causes, mechanism and control of cracking in concrete", SP-20 American Concrete Institute, Detroit, 87-117.

Hassan, A.S. (2008), "Crack control for reinforced concrete members subjected to flexure", Master of Science Thesis, Alexandria University, Alexandria, Egypt.

Johnson, A.I. (1951), "Deformation of reinforced concrete", *Int. Assoc. Bridge Struct. Eng. Publ.*, **11**, 253-290.

Kang, S.B., Tan, K.H., Zhou, X.H. and Yang, B. (2017), "Influence of reinforcement ratio on tension stiffening of reinforced engineered cementitious composites", *Eng. Struct.*, **141**, 251-261.

Korean Highway Bridge Specifications (2012), Korean Ministry of Construction and Transportation.

Lee, J.H., Ho, H.N., Shinozuka, M. and Lee, J.J. (2012), "An advanced bision-based system for real-time displacement measurement of high-rise buildings", *Smart Mater. Struct.*, **21**, 1-10.

Lee, J.H., Jung, C.Y., Choi, E. and Cheung, J.H. (2017), "Vision-based multipoint measurement systems for structural in-plane and out-of-plane movements including twisting rotation", *Smart Struct. Syst.*, **20**(5), 563-572.

Lee, S.C., Cho, J.Y. and Vecchio, F.J. (2011), "Model for post-yield tension stiffening and rebar rupture in concrete members", *Eng. Struct.*, **33**, 1723-1733.

Lee, S.C., Cho, J.Y. and Vecchio, F.J. (2013), "Tension-stiffening model for steel fiber-reinforced concrete containing conventional reinforcement", *Am. Concrete Inst.: Struct. J.*, **110**, 639-648.

Leonhardt, F. (1977), "Crack control in concrete structures", IABSE Surveys, No.S4/77, International Association for Bridges and Structural Engineering, Zurich.

Lin, C.W., Hsu, W.K., Chiou, D.J., Chen, C.W. and Chiang, W.L. (2015), "Smart monitoring system with multi-criteria decision using a feature based computer vision technique", *Smart Struct. Syst.*, **15**, 1583-1600.

Mondal, T.G. and Prakash, S.S. (2015), "Effect of tension stiffening on the behaviour of reinforced concrete circular columns under torsion", *Eng. Struct.*, **92**, 186-195.

Scanlon, A. and Murray, D.W. (1974), "Time-dependent reinforced concrete slab deflections", *J. Struct. Div.*, ASCE, **100**, 1911-1924.

Scott, R.H. and Beeby, A.W. (2012), "Evaluation and management of tension stiffening", *Am. Concrete Inst.: Spec. Publ.*, **284**, 1-18.

Structural Use of Concrete (1997), Code of Practice for Design and Construction, British Standards Institution: UK.

Watstein, D. and Parsons, D.E. (1943), "Width and spacing of tensile cracks in axially reinforced concrete cylinders", *J. Res. Nat. Bureau Stand.*, **31**, 1-24.

Welch, G.B. and Janjua, M.A. (1971), "Width and spacing of tensile cracks in reinforced concrete", UNICIV Report No R76, University of NSW, Kensington.

Yankelevsky, D.Z., Jabareen, M. and Abutbul, A.D. (2008), "One-dimensional analysis of tension stiffening in reinforced concrete with discrete cracks", *Eng. Struct.*, **30**, 206-217.

Ye, X.W., Dong, C.Z. and Liu, T. (2016), "Force monitoring of steel cables using vision-based sensing technology: methodology and experimental verification", *Smart Struct. Syst.*, **18**, 585-599.

Ye, X.W., Ni, Y.Q., Wai, T.T., Wong, K.Y., Zhang, X.M. and Xu, F. (2013), "A vision-based system for dynamic displacement measurement of long-span bridges: algorithm and verification", *Smart Struct. Syst.*, **12**, 363-379.

*CC*